1-8-2017

# Numerical Simulation of Acoustic Emission During Crack Growth in 3-point Bending Test

Mihhail Berezovski
*Embry-Riddle Aeronautical University*, berezovm@erau.edu

Arkadi Berezovski
*Laboratory of Nonlinear Dynamics, Institute of Cybernetics at Tallinn University*



## Scholarly Commons Citation
Berezovski A, Berezovski M. Numerical simulation of acoustic emission during crack growth in 3-point bending test. Struct Control Health Monit. 2017;24:e1996. https://doi.org/10.1002/stc.1996

Received: 16 August 2016 | Revised: 16 November 2016 | Accepted: 8 January 2017
DOI: 10.1002/stc.1996

WILEY

RESEARCH ARTICLE

# Numerical simulation of acoustic emission during crack growth in 3-point bending test

**A. Berezovski**[1] | **M. Berezovski**[2]

[1]Laboratory of Nonlinear Dynamics, Institute of Cybernetics at Tallinn University of Technology, 21 Akadeemia Rd. Tallinn, 12618, Estonia
[2]Department of Mathematics, Embry-Riddle Aeronautical University, 600 South Clyde Morris Blvd. Daytona Beach 32114-3900, FL, USA

**Correspondence**
A. Berezovski, Laboratory of Nonlinear Dynamics, Institute of Cybernetics at Tallinn University of Technology, 21 Akadeemia Rd., Tallinn 12618, Estonia.
Email: berez@ioc.ee

**Funding information**
EU through the European Regional Development Fund Estonian Research Council, Grant/Award Number: PUT434

**Summary**
Numerical simulation of acoustic emission by crack propagation in 3-point bending tests is performed to investigate how the interaction of elastic waves generates a detectable signal. It is shown that the use of a kinetic relation for the crack tip velocity combined with a simple crack growth criterion provides the formation of waveforms similar to those observed in experiments.

**KEYWORDS**
acoustic emission, dynamic crack, numerical simulation, wave propagation

## 1 | INTRODUCTION

Acoustic emission (AE) is widely applied in the structural health monitoring to detect individual fracture events.[1–3] One of the main sources of acoustic emission is a crack propagating in a material. Elastic waves radiated due to the moving crack tip that create a signal, which can be recognized by detectors. The problem of elastic wave propagation from a moving source inside a body can be solved numerically, at least in principle. However, numerical simulations of acoustic emission do not fully capture the wave phenomena occurring during dynamic crack propagation.[4] This relates to the complexity in the dynamic crack propagation.[5] In the framework of the continuum description, a crack path and its tip velocity are the two problematic issues. Whereas the crack path can be aligned by boundary conditions, the crack tip velocity should be determined by a kinetic relation.[6]

To understand the connection between acoustic emission and crack propagation in more detail, we simulate numerically the well-known 3-point bending test embedding a simple model for the crack tip velocity.[7, 8] The fracture in the 3-point bending test is in the opening mode (Mode 1) of loading, and the crack path can be assumed as a straight line. Such simplified description of crack propagation is used as a sample for more complicated situations. The purpose of the paper is to study the ability of the proposed model to reproduce the AE signal as the result of the interaction of elastic waves radiated by the propagating crack. Calculations are performed by means of the conservative finite-volume wave-propagation algorithm, which was proposed in previous studies[9, 10] and modified for the application to front propagation in other studies.[11–13] The algorithm was successfully applied to wave propagation simulations in inhomogeneous solids.[14] Here, the algorithm is specified for the accounting of a moving crack in two dimensions.

The paper is organised as follows. After a brief explanation of the 3-point bending test in Section 1, the governing equations of the plane strain elasticity are recalled in Section 2. The method of calculation of the dynamic $J$-integral is described in Section 3. Section 4 is devoted to the kinetic relation for the straight brittle crack. The numerical procedure, initial and boundary conditions, and material parameters are presented in Section 5. Results of the numerical simulations are discussed in the last Section of the paper.

## 2 | 3-POINT BENDING TEST

It should be noted that the single edge V-notched beam (SEVNB) method is the standard method for evaluating the fracture toughness.[15, 16] In the SEVNB method, the standard bend specimen is a single edge-notched and fatigue-cracked beam loaded in 3-point bending with a support span, $S$, nominally equal to four times the width, $W$. The general proportions of the specimen configuration are shown in Figure 1.

  

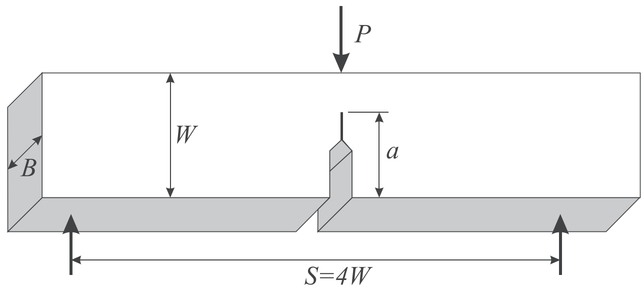


**FIGURE 1** Specimen geometry

The basic procedure involves loading a specimen to a selected displacement level and determining the amount of crack extension that occurred during loading.[17]

The stress intensity, $K_I$, represents the level of stress at the tip of the crack and the fracture toughness, and $K_{Ic}$ is the highest value of stress intensity that a material under specific (plane–strain) conditions can withstand without fracture. As the stress intensity factor reaches the $K_{Ic}$ value, unstable fracture occurs.

For isotropic, perfectly brittle, linear-elastic materials, the fracture toughness can be directly related to the $J$-integral if the crack extends straight ahead with respect to its original orientation. For plane strain under Mode 1 loading conditions,[6]

$$J = K_I^2 \frac{1 - \nu^2}{E}, \tag{1}$$

where $E$ is the elastic modulus and $\nu$ is Poisson's ratio.

## 3 | PLANE STRAIN ELASTICITY

Numerical simulation of the crack propagation in the 3-point bending test is based on the solution of equations of two-dimensional linear elasticity. Neglecting both geometrical and physical nonlinearities, we can write the bulk equations of homogeneous linear isotropic elasticity in the absence of body force as follows[18]:

$$\rho \frac{\partial v_i}{\partial t} = \frac{\partial \sigma_{ij}}{\partial x_j}, \tag{2}$$

$$\frac{\partial \sigma_{ij}}{\partial t} = \lambda \frac{\partial v_k}{\partial x_k} \delta_{ij} + \mu \left( \frac{\partial v_i}{\partial x_j} + \frac{\partial v_j}{\partial x_i} \right), \tag{3}$$

where $t$ is the time, $x_j$ is the spatial coordinate, $v_i$ is the component of the velocity vector, $\sigma_{ij}$ is the Cauchy stress tensor, $\rho$ is the density, and $\lambda$ and $\mu$ are the Lamé coefficients.

Consider a sample that is relatively thick along $x_3$ and where all applied forces are uniform in the $x_3$ direction. Because all derivatives with respect to $x_3$ vanish, all fields can be viewed as functions of $x_1$ and $x_2$ only. This situation is called plane strain. The corresponding displacement component (e.g., the component $u_3$ in the direction of $x_3$) vanishes, and the others $(u_1, u_2)$ are independent of that coordinate $x_3$; that is,

$$u_3 = 0, \quad u_i = u_i(x_1, x_2), \quad i = 1, 2. \tag{4}$$

It follows that the strain tensor components, $\epsilon_{ij}$, are

$$\epsilon_{i3} = 0, \quad \epsilon_{ij} = \frac{1}{2}(u_{i,j} + u_{j,i}), \quad i,j = 1, 2. \tag{5}$$

The stress components follow then

$$\sigma_{3i} = 0, \quad \sigma_{33} = \frac{E}{1 - 2\nu} \left( \frac{\nu}{1 + \nu} \epsilon_{ii} \right), \quad i = 1, 2, \tag{6}$$

$$\sigma_{ij} = \frac{E}{1 + \nu} \left( \epsilon_{ij} + \frac{\nu}{1 - 2\nu} \epsilon_{kk} \delta_{ij} \right), \quad i, j, k = 1, 2, \tag{7}$$

where $E$ is Young's modulus, $\nu$ is Poisson's ratio, and $\delta_{ij}$ is the unit tensor.

Inversion of Equation 7 yields an expression for the strains in terms of stresses:

$$\epsilon_{ij} = \frac{1 + \nu}{E} \left( \sigma_{ij} - \nu \sigma_{kk} \delta_{ij} \right), \quad i, j, k = 1, 2. \tag{8}$$

To simulate the crack propagation, we need to apply a criterion for crack growth. We use the simple Griffith criterion[19]: When applied loading is such that

$$K_I \geqslant K_{Ic}, \tag{9}$$

then the crack will grow. The same criterion can be expressed in terms of the energy release rate ($J$-integral), because of relation (Equation 1)

$$J \geqslant J_c. \tag{10}$$

The $J$-integral is path independent, which allows to calculate it as explained below.

### 3.1 | Dynamic *J*-integral

The dynamic $J$-integral for a homogeneous cracked body has the physical meaning of the energy release rate.[20–22] It can be expressed in the case of Mode 1 straight crack as follows:

$$J = \lim_{\Gamma \to 0} \int_\Gamma \left( (W + K)\delta_{2j} - \sigma_{ij} \frac{\partial u_i}{\partial x_2} \right) n_j d\Gamma. \tag{11}$$

Here, $x_2$ is the coordinate in the direction of applied loading, and $n_j$ is the unit vector normal to an arbitrary contour $\Gamma$ pointing outward of the enclosed domain (see Figure 2).

The specific elastic energy stored in the body, $W$, and kinetic energy density, $K$, in a linear elastic medium are given by

$$W = \frac{1}{2} \sigma_{ij} \epsilon_{ij}, \quad K = \frac{1}{2} \rho v_i^2. \tag{12}$$

A domain integral representation of $J$ is more suited for numerical computation.[23, 24] Following the work of Moran and Shih,[24] a weighting function $q$ is introduced, which has

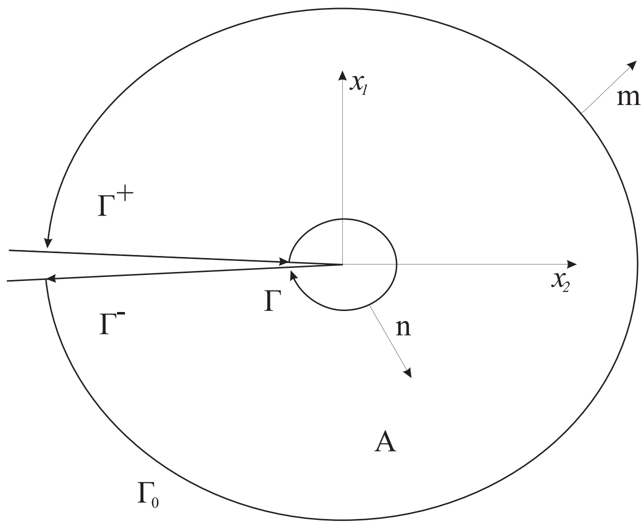


**FIGURE 2** Crack tip coordinates and integration contours

a value of unity on the inner contour Γ and zero on the outer contour $\Gamma_0$. Within the enclosed area $A$, $q$ is an arbitrary smooth function of $x_1$ and $x_2$ with values ranging from zero to one.

Using the weighting function $q$, Equation (11) can be rewritten in the form:

$$J = \lim_{\Gamma\to 0}\left(-\int_C H_{2j} m_j q\, dC + \int_{\Gamma^+ + \Gamma^-} H_{2j} m_j q\, dC\right), \tag{13}$$

where $C = \Gamma + \Gamma^+ + \Gamma^- + \Gamma_0$, vector $m_j$ denotes the unit vector normal to $C$, pointing outward from the enclosed area $A$, and

$$H_{2j} = (W + K)\delta_{2j} - \sigma_{ij}\frac{\partial u_i}{\partial x_2}. \tag{14}$$

Components of the function $H$ are

$$H_{21} = (W + K)\delta_{21} - \sigma_{i1}\frac{\partial u_i}{\partial x_2} = -\sigma_{11}\frac{\partial u_1}{\partial x_2} - \sigma_{21}\frac{\partial u_2}{\partial x_2}. \tag{15}$$

$$\begin{aligned} H_{22} &= (W + K)\delta_{22} - \sigma_{i2}\frac{\partial u_i}{\partial x_2} = \\ &= (\frac{1}{2}\sigma_{1j}\epsilon_{1j} + \frac{1}{2}\sigma_{2j}\epsilon_{2j} + \frac{1}{2}\rho(v_1^2 + v_2^2)) - \sigma_{12}\frac{\partial u_1}{\partial x_2} - \sigma_{22}\frac{\partial u_2}{\partial x_2} = \\ &= (\frac{1}{2}\sigma_{11}\epsilon_{11} + \frac{1}{2}\sigma_{12}\epsilon_{12} + \frac{1}{2}\sigma_{21}\epsilon_{21} + \frac{1}{2}\sigma_{22}\epsilon_{22} + \frac{1}{2}\rho(v_1^2 + v_2^2)) \\ &\quad - \sigma_{12}\frac{\partial u_1}{\partial x_2} - \sigma_{22}\frac{\partial u_2}{\partial x_2}. \end{aligned} \tag{16}$$

Applying the divergence theorem, the contour integral in Equation (13) can be converted into an equivalent domain form[24]:

$$\begin{aligned} J &= -\int_A \left(H_{2j}\frac{\partial q}{\partial x_j} + \frac{\partial H_{2j}}{\partial x_j} q\right) dA = \\ &= -\int_A \left(H_{21}\frac{\partial q}{\partial x_1} + H_{22}\frac{\partial q}{\partial x_2} + \frac{\partial H_{21}}{\partial x_1} q + \frac{\partial H_{22}}{\partial x_2} q\right) dA. \end{aligned} \tag{17}$$

The integral over $\Gamma^+ + \Gamma^-$ vanishes because of traction-free crack surfaces.

The effect of the choice of a $q$ function on the calculated $J$ values is not significant.[25] In this paper, a "bell" type $q$ function is used

$$q(x_1, x_2) = \exp(-x_1^2/b - (x_2 - a)^2/c). \tag{18}$$

where $a$ is the position of the crack tip, and $b$ and $c$ are parameters.

## 4 | VELOCITY OF THE CRACK IN MODE 1

To simulate crack propagation, we need to determine the crack tip velocity. In the numerical procedure, we can estimate the velocity at any time step by means of the jump relation associated with the bulk equation for linear momentum[26, 27]:

$$V_C[\rho\bar{v}_i] + N_j[\bar{\sigma}_{ij}] = 0, \tag{19}$$

where overbars denote the values averaged over a computational cell, square brackets denote jumps, and $N_j$ is the normal to the crack front. The material velocity $V_j$ is connected with the physical velocity $v_i$ by[28]

$$\bar{v}_i = -(\delta_{ij} + \frac{\partial \bar{u}_i}{\partial x_j})V_j. \tag{20}$$

Inserting the latter relation into former one, we have

$$V_C\left[\rho(\delta_{ij} + \frac{\partial \bar{u}_i}{\partial x_j})V_j\right] - N_j[\bar{\sigma}_{ij}] = 0. \tag{21}$$

In the case of a straight crack in Mode 1, the last expression reduces to

$$V_C^2 = \frac{\bar{\sigma}_{22}}{\rho(1 + \bar{\epsilon}_{22})}, \tag{22}$$

where $V_C$ is the crack tip velocity and $\sigma_{22}$ and $\epsilon_{22}$ are stress and strain components in the direction of the crack propagation, respectively.

These stress and strain components at the crack tip are not determined due to the square root singularity. As it is shown,[7] if we apply a local equilibrium approximation for $\sigma_{22}$ and linear stress-strain relation for $\epsilon_{22}$, we will arrive at the kinetic relation

$$\frac{V_C^2}{c_R^2} = \frac{\bar{\sigma}_{22}}{\bar{\sigma}_{22} + \rho_0 c_R^2}, \tag{23}$$

with the Rayleigh velocity $c_R$ as the limiting crack tip velocity. Here, $\bar{\sigma}_{22}$ is the local equilibrium (averaged) value of the stress component.

As experiments show,[29] the limiting velocity of the crack tip is usually significantly less than the Rayleigh speed. This leads to a generalization of the kinetic relation (Equation 23) by introducing a limiting crack speed $V_T$

$$\frac{V_C^2}{V_T^2} = \frac{\sigma_{22}}{\sigma_{22} + \rho_0 V_T^2}, \tag{24}$$

but the stress component $\sigma_{22}$ at the crack tip is no more an equilibrium one. To determine its value, we apply an assumption analogous to that in the case of the phase boundary[8]

$$\sigma_{22} = N f_C, \tag{25}$$

where $f_C$ is the driving force acting at the crack tip and $N$ is a material dependent coefficient.

In the thin strip geometry, the driving force is related to the $J$-integral (e.g., Maugin[30])

$$f_C = \frac{J}{l}, \tag{26}$$

where $l$ is a scaling factor with dimension of length.

Accordingly, we arrive at the kinetic relation

$$\frac{V_C^2}{V_T^2} = \frac{NJ/l}{NJ/l + \rho_0 V_T^2} = 1 - \left( \frac{1}{1 + NJ/\rho_0 V_T^2 l} \right). \tag{27}$$

The characteristic length $l$ can be related to the process zone length[31]

$$l \sim \frac{K_{Ic}^2}{\sigma_f^2}, \tag{28}$$

with the critical value of the stress intensity factor $K_{Ic}$ and the applied stress $\sigma_f$.

The value of the applied stress $\sigma_f$, in its turn, can be expressed in terms of the dynamic release rate (Equation 1). Correspondingly, the kinetic relation (Equation 27) can be rewritten as (cf. Berezovski and Maugin[7])

$$\frac{V_C^2}{V_T^2} = 1 - \left( 1 + M \frac{J^2}{J_c} \right)^{-1}, \tag{29}$$

where the coefficient $M$ depends on the properties of material.

## 5 | NUMERICAL SIMULATION OF CRACK PROPAGATION

To compute the value of the $J$-integral by means of Equations 14–18, we need to know the strain and stress fields. For this purpose, system of Equations 2 and 3, specialized to plane strain conditions by Equations 4–8, is solved numerically by means of the conservative finite-volume wave-propagation algorithm. The advantages of the wave-propagation algorithm are its stability up to the Courant number equal to unity, high-order accuracy, and energy conservation.[10] It should be noted that discrete element method, which is the basis of lattice model simulations (see Birck et al.,[32] e.g.), provides equivalent results for continuum dynamic problems, as shown in the work of K. and W. Liu.[33]

The corresponding two-dimensional computational domain is shown in Figure 3.

Loading is applied at the middle of the upper boundary. Initial crack is placed at the middle of the bottom. Boundaries are stress free except the left and right ends of the bottom boundary, which are fixed. Initially, the beam is at rest yielding zero initial values of wanted fields on all cells. The solution includes two steps. First, numerical fluxes at boundaries between cells are computed. Then new averaged stresses, strains and velocities on all cells are evaluated. Their values at the boundaries are computed using boundary conditions. The solution procedure is described in detail in the work of Berezovski et al.[14]

The size of the beam is chosen as follows: length $S = 250$ mm, height $W = 60$ mm, width $B = 30$ mm. Silica aerogel is chosen as the material of the beam. Its properties are extracted from the work of Phalippou et al.[34]: the density $\rho$ is 200 kg/m$^3$), Young's Modulus $E$ is 6.5 MPa, Poisson's ratio is 0.2, and the fracture toughness $K_c$ is 2 KPa-m$^{1/2}$.

For numerical simulation, the space step $\Delta x$ is chosen as 1 mm, and the corresponding time step is determined from the value of the Courant number equal to 1. This gives the value of the time step as $\Delta t = \Delta x / c_p$. In the case of silica aerogel $c_p = 80$ m/s, which results in the value of the time step $\Delta t = 0.510^{-5}$ s. The loading is determined by the cross-head velocity, which constant value is chosen as 0.294 m/s. The time history of the loading in terms of the normalized stress in the middle of the upper boundary is presented in Figure 4. The loading is eliminated at 4,000 time steps to avoid the complete breaking down of the specimen.

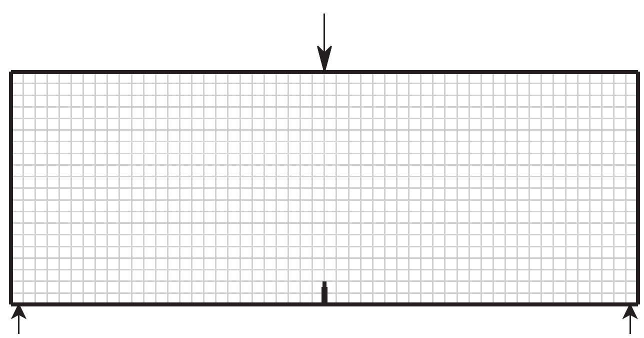

**FIGURE 3** Sketch of computational domain

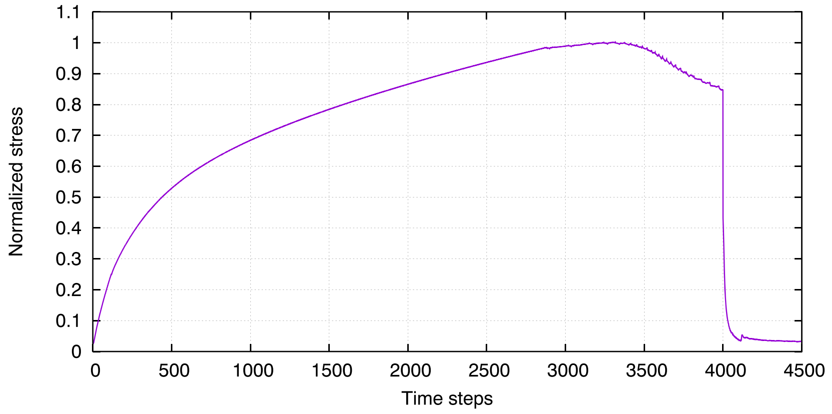


**FIGURE 4** Load time history

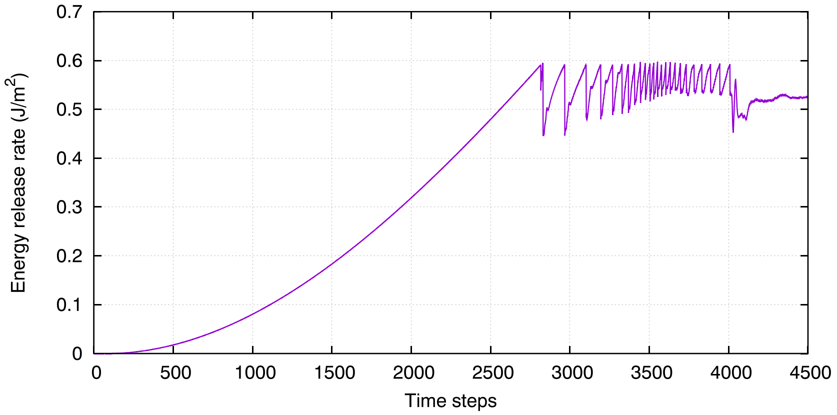


**FIGURE 5** Time history of the energy release rate

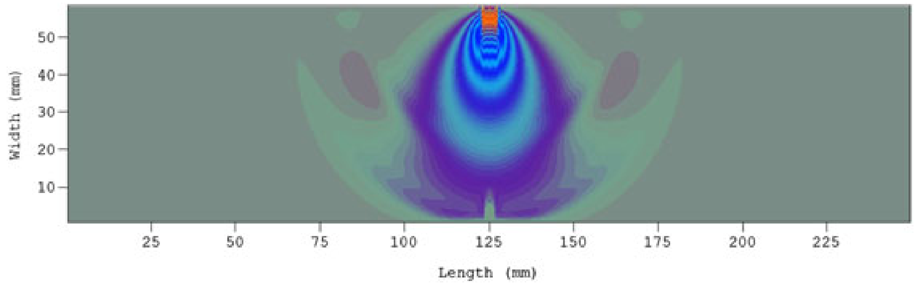


**FIGURE 6** Stress field at 60 time steps

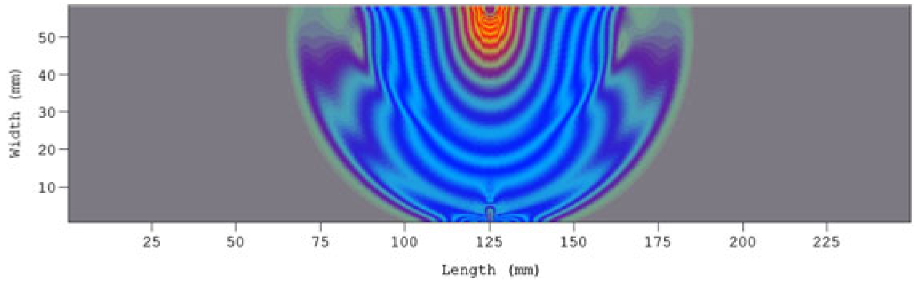


**FIGURE 7** Wave field at 60 time steps

The value of the *J*-integral is computed by means of Equations 14–18 at every time step. If this value overcomes its critical value, then the crack starts to propagate. The velocity of the crack propagation is calculated by means

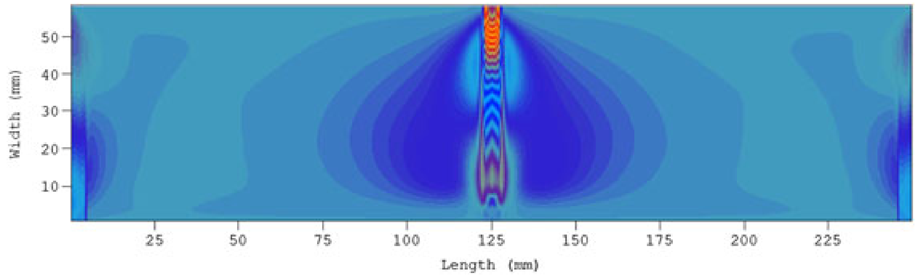


**FIGURE 8** Stress field at 1600 time steps

of Equation 29 with the value of dimensionless coefficient $M = 0.375$. A simple procedure for the tracking of the crack tip is applied. Its virtual displacement is computed for each time step. We keep the location of the crack tip in the old place if the sum of its virtual displacements is less than the size of space step, and change it to one space step forward otherwise. All the calculations are performed with the Courant number equal to 1.

## 6 | RESULTS AND DISCUSSION

Time history of the $J$-integral presented in Figure 5 shows that initially, its value is increased with time like a square of time. The crack starts to grow if the critical value of the $J$-integral is reached. The crack growth is accompanied by a sudden decrease of the value of the $J$-integral due to the stress relaxation. It means that the crack is not growing until the value of the $J$-integral could reach its critical value again. The process is repeating until 4,000 time steps; after that the loading is eliminated. The similar discontinuous behavior of the crack in the 3-point bending test is mentioned in the work of Carpinteri et al.[35]

Typical wave propagation from a point source in the middle of the upper boundary is observed for first 500 time steps. As an example, normal stress distribution and wave field (in fact, the energy distribution) for 60 steps are given in Figures 6 and 7. Then a stabilized wave field is formed and kept for next 2,300 time steps. The corresponding normal stress distribution and wave field for 1,600 time steps are shown in Figures 8 and 9.

The crack starts to grow approximately at 2,815 time steps that is reflected in the radiation of short waves from the crack tip. The interaction of these radiated waves with the global wave field established before is displayed in supplementary animated picture, which shows the evolution of wave field from 2,800 till 4,000 time steps as well as the crack propagation. The growing size of the crack is also clearly seen. Typical example of normal stress distribution at 4,000 time steps is given in Figure 10.

Waves emitted by the growing crack due to their interference and reflection from boundaries form the wave pattern

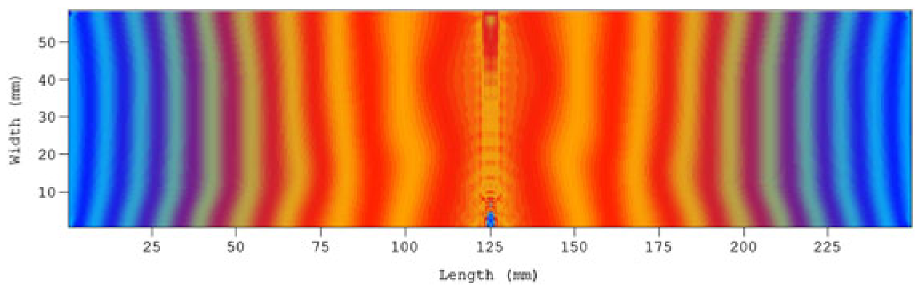


**FIGURE 9** Wave field at 1600 time steps

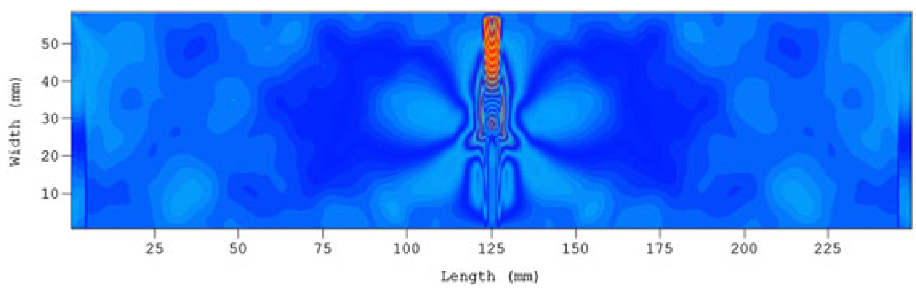


**FIGURE 10** Stress field at 4000 time steps

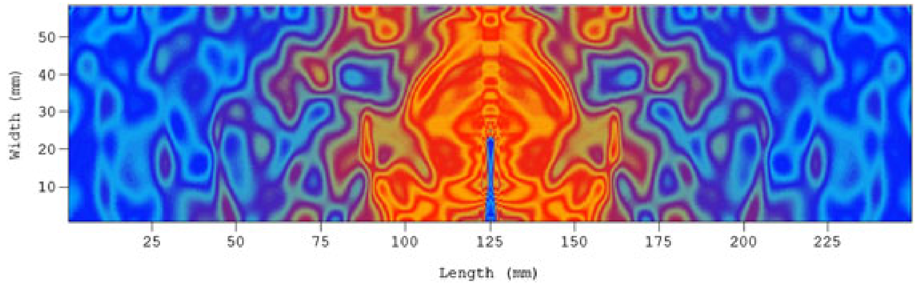


**FIGURE 11** Wave field at 4000 time steps

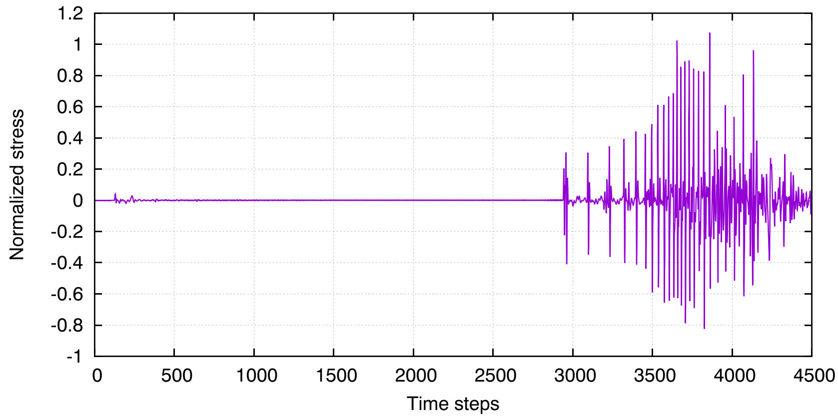


**FIGURE 12** Time history of the normal stress at the boundary

shown in Figure 11. In the middle of the side boundaries, they generate a signal presented in Figure 12 in terms of the normal stress. This waveform looks qualitatively similar to those registered in experiments.[36] This means that numerical simulation of the crack propagation under the 3-point bending test conditions can predict acoustic emission even in the framework of a simple macroscopic model for the crack tip velocity. Despite the simplified representation of the fracturing process, it provides the possibility to calculate the signal as a result of interaction of elastic waves. The 3-point bending test is chosen for the numerical simulation because it is the standard procedure for the determination of the fracture toughness of materials.

It should be noted that the dissipation of energy due to the crack propagation is controlled by the velocity of the crack tip and the driving force (the energy release rate). The applied numerical procedure of the crack tip tracking provides only an estimate of the dissipated energy. A more accurate discontinuity tracking procedure with the mesh adaptation is needed for more detailed results. Such a procedure, which is crucial for a nonstraight crack path, is under development.

## ACKNOWLEDGMENTS

The research was supported by the EU through the European Regional Development Fund and by the Estonian Research Council (Grant PUT434).

## REFERENCES

[1] C. U. Grosse, M. Ohtsu, *Acoustic Emission Testing*, Springer, Berlin, Heidelberg **2008**.

[2] K. Ono. *J. of Acoust. Emission* **2011**, *29*, 284.

[3] K. Ono, A. Gallego. *J. of Acoust. Emission* **2012**, *30*, 180.

[4] A. Lisjak, Q. Liu, Q. Zhao, O. K. Mahabadi, G. Grasselli. *Geophys. J. Int.* **2013**, *195*(1), 423.

[5] J. Fineberg, E. Bouchbinder. *Int. J. of Fracture* **2015**, *196*(1–2), 33.

[6] L. B. Freund, *Dynamic Fracture Mechanics*, Cambridge University Press, Cambridge, UK **1998**.

[7] A. Berezovski, G. A. Maugin. *Int. J. of Fracture* **2007**, *143*(2), 135.

[8] A. Berezovski, G. A. Maugin. *ZAMM-J. of Appl. Math. and Mechanics/Zeitschrift für Angewandte Mathematik und Mechanik* **2010**, *90*(7–8), 537.

[9] R. J. LeVeque. *J. Comput. Phys.* **1997**, *131*(2), 327.

[10] R. J. LeVeque, *Finite Volume Methods for Hyperbolic Problems*, Cambridge University Press, Cambridge, UK **2002**.

[11] A. Berezovski, J. Engelbrecht, G. A. Maugin. *Arch. of Appl. Mech.* **2000**, *70*(10), 694.

[12] A. Berezovski, G. A. Maugin. *J. of Comput. Phys.* **2001**, *168*(1), 249.

[13] A. Berezovski, G. A. Maugin. *J. of Thermal Stresses* **2002**, *25*(8), 719.

[14] A. Berezovski, J. Engelbrecht, G. A. Maugin, *Numerical Simulations of Waves and Fronts in Inhomogeneous Solids*, World Scientific, Singapore **2008**.

[15] R. Morrell. *Adv. in Appl. Ceramics* **2006**, *105*(2), 88.

[16] J. Xu, D. Tang, K.-J. Lee, H.-B. Lim, K. Park, W.-S. Cho. *J. of Ceramic Process. Res.* **2012**, *13*(6), 683.

[17] 2011e1 ASTM Standard E1820, *Standard Test Method for Measurement of Fracture Toughness*, ASTM International, West Conshohocken, PA **2011**.

[18] J. R. Barber, *Elasticity*, Springer, Dordrecht **2009**.

[19] A. T. Zehnder, *Fracture Mechanics*, Springer, London **2012**.

[20] C. Atkinson, J. D. Eshelby. *Int. J. of Fracture Mech.* **1968**, *4*(1), 3.

[21] L. B. Freund. *J. of Elasticity* **1972**, *2*(4), 341.

[22] G. A. Maugin. *Acta Mech.* **1994**, *105*(1–4), 33.

[23] T. Nakamura, CF. Shih, L. B. Freund. *Int. J. of Fracture* **1985**, *27*(3–4), 229.

[24] B. Moran, C. F. Shih. *Int. J. of Fracture* **1987**, *35*(4), 295.

[25] C. F. Shih, B. Moran, T. Nakamura. *Int. J. of Fracture* **1986**, *30*(2), 79.

[26] G. A. Maugin. *ARI-An Int. J. for Physical and Eng. Sci.* **1997**, *50*, 41.

[27] G. A. Maugin. *ARI-An Int. J. for Phys. and Eng. Sci.* **1998**, *50*(3), 141.

[28] G. A. Maugin, *Material Inhomogeneities in Elasticity*, Chapman and Hall, London: **1993**.

[29] K. Ravi-Chandar, *Dynamic Fracture*, Elsevier Amsterdam **2004**.

[30] G. A. Maugin. *Arch. of Appl. Mech.* **2000**, *70*(1–3), 31.

[31] H. Awaji, Y. Nishimura, S.-M. Choi, Y. Takahashi, T. Goto, S. Hashimoto. *J. of the Ceramic Soc. of Japan* **2009**, *117*(1365), 623.

[32] G. Birck, I. Iturrioz, G. Lacidogna, A. Carpinteri. *Eng. Failure Anal.* **2016**, *70*, 157.

[33] K. Liu, W. Liu. *Arch. of Appl. Mech.* **2006**, *76*(3), 229.

[34] J. Phalippou, T. Woignier, R. Rogier. *Le J. de Phys. Colloques* **1989**, *50*(C4), 191.

[35] A. Carpinteri, G. Lacidogna, M. Corrado, E. Di Battista. *Eng. Fracture Mech.* **2016**, *155*, 130.

[36] T. Kishi, M. Ohtsu, S. Yuyama, *Acoustic Emission-Beyond the Millennium*, Elsevier, Amsterdam **2000**.

## SUPPORTING INFORMATION

Additional Supporting Information may be found online in the supporting information tab for this article.

**How to cite this article:** Berezovski A, Berezovski M. Numerical simulation of acoustic emission during crack growth in 3-point bending test. *Struct Control Health Monit*. 2017;24:e1996. https://doi.org/10.1002/stc.1996